Research Article | Vol. 31, No. 21 / 9 Oct 2023 / Optics Express 35218
Optics EXPRESS

Demonstration of a highly efficient topological vertical coupler

Sho Okada,[1,4] Hibiki Kagami,[1,2] Nobuhiko Nishiyama,[1] Xiao Hu,[3] and Tomohiro Amemiya[1,5]

[1]Department of Electrical and Electronic Engineering, Tokyo Institute of Technology, Tokyo 152-8552, Japan
[2]Current address: NTT Device Technology Laboratories, Kanagawa-ken 243-0198, Japan
[3]Research Center for Materials Nanoarchitectonics (MANA), National Institute for Materials Science (NIMS), Ibaraki 305-0044, Japan
[4]okada.s.ah@m.titech.ac.jp
[5]amemiya.t.ab@m.titech.ac.jp

Abstract: A defect structure is proposed for enhancing the coupling efficiency of vertically incident circularly polarized light in a topological waveguide. In the topological edge-state waveguide based on triangle lattices of hexagons consisting of six nanoholes respecting C_{6v} symmetry in a silicon optical circuit, the vertical coupling rate is improved by removing the nanoholes from one hexagonal cell near the line. The coupling efficiency was evaluated with and without the defect structure. The introduced defect structure operates suitably for focused beams of left- and right-handed circularly polarized light, enhancing the optical communication wavelength bandwidth by up to 10 dB.

1. Introduction

Topological physical phenomena have attracted significant attention from researchers in recent years. The expectations for the discovery of new physics associated with topologically protected surface states and the development of devices using such phenomena are constantly increasing [1–3]. Therefore, recent investigations have focused on topological photonics, which traces the topology of electronic systems to that of photonic systems [4–6]. Topological photonic systems are characterized by the ability to realize photonic structures distinct in topology by simultaneously controlling the interactions within and between the cells in photonic nano-periodic structures. This enables more flexible photonic band engineering than is observed in conventional photonic crystals [7–10], which primarily involve cell-to-cell interactions, and metamaterials [11–17], which involve intra-cell interactions.

One of the most attractive phenomena in topological photonic systems is the topological edge state generated at the interface of two photonic structures distinct in topology, whereby the direction of the propagating light is uniquely determined with respect to the spin direction (i.e., left or right circular polarization) [18–21]. This means that vertically incident light can be automatically split according to the type of circular polarization [19,22], which can be an important element toward a fully passive demultiplexer in optical polarization multiplexing system [23]. However, the modes of circular polarized light propagating in free space and light propagating in a topological waveguide are significantly different, and it is not easy to achieve high vertical coupling efficiency while maintaining chiral coupling performance. Therefore, until now, no versatile structure has been proposed to realize highly efficient vertical coupling from free space to topological waveguides.

With the above background, we reported that a high vertical coupling rate can be obtained by introducing a defect structure close to the topological waveguide [24]. In this study, we fabricated an actual device based on the previous proposal and evaluated its vertical coupling rate. The

#500091 https://doi.org/10.1364/OE.500091
Journal © 2023 Received 31 Jul 2023; revised 13 Sep 2023; accepted 13 Sep 2023; published 5 Oct 2023

Optics EXPRESS

details of the experimental analysis and the corresponding findings are described in subsequent sections.

2. Device fabrication and experimental analysis

Figure 1 depicts the structure of the device used in this study. We employed triangle lattices of hexagons consisting of six nanoholes respecting C_{6v} symmetry on a silicon-on-insulator (SOI) wafer as a photonic structure with Z_2 topology. A topological waveguide was then constructed by combining two photonic structures with distinct topologies. Additionally, to improve the vertical coupling rate, the triangular nanoholes were removed from a specific triangle lattice of hexagons near the topological waveguide; hereafter, this arrangement is referred to as the "defect structure." The triangle lattices of hexagons in the defect structure was filled with a dielectric material exhibiting a high refractive index to form a cavity; the vertically incident light could be strongly confined in this cavity. In our previous reports [24], we predicted that by introducing a defect structure at a specific location near the topological waveguide as shown in Fig. 1(a), the confined light can be easily coupled to a topological waveguide that exhibits high efficiency. In this situation, the mode distribution inside the defect is almost the same as that of a plane wave with circular polarization focused by a lens. This mode matching facilitates an efficient conversion from the circularly polarized beam propagating in free space to the guided wave passing through the topological waveguide.

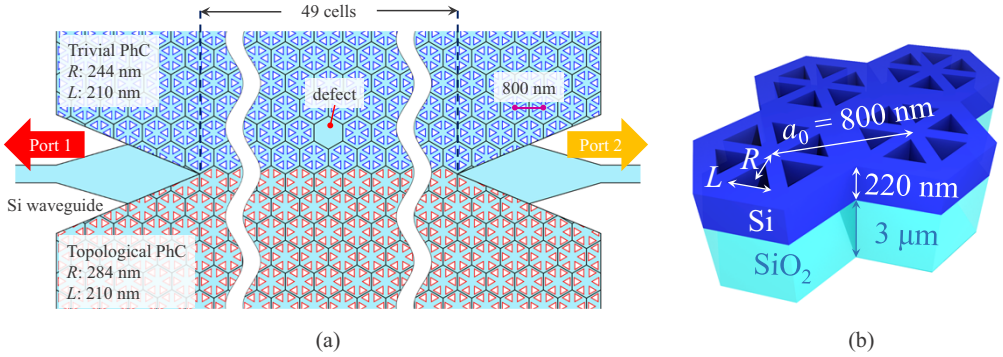

Fig. 1. (a) Schematic of the topological vertical coupler with the defect structure. (b) Unit cell of a topological photonic crystal.

During device fabrication, ZEP520A (film thickness: 500 nm) was applied on the SOI substrate, with the Si core thickness and the SiO_2 cladding thickness set to 220 nm and 3 μm, respectively. Subsequently, a device pattern was formed using electron beam lithography. The ZEP520A was used as a mask, and the Si layer was etched by inductively coupled reactive ion etching using SF_6 mixed gas. The period a_0 of the honeycomb lattice and the length L of one side of the nanohole were set to 800 and 210 nm, respectively. Two photonic structures distinct in topology were implemented by changing only the distance R from the center of the triangle lattices of hexagons to that of the nanohole. Based on the band structure analysis performed using the plane wave expansion method and various experimental rules [25], we employed two structures with $R = 244$ and 284 nm. The band gaps in these two topological photonic structures were close to the C-band.

Figure 2(a) depicts an optical microscope image of the fabricated device. Figure 2(b) shows a scanning electron microscope image with the area surrounded by the yellow dotted line in Fig. 2(a) enlarged. These images reveal that the values of the aforementioned device parameters are close to the described design with the defect structure appropriately fabricated. Furthermore, a topological converter [26] was inserted to increase the coupling efficiency between the topological waveguide and the silicon wire waveguide.

Optics EXPRESS

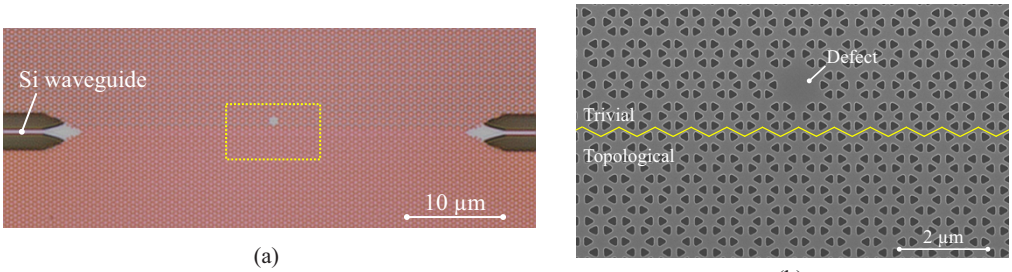

Fig. 2. (a) Optical microscope image of the topological vertical coupler with the defect structure. (b) Scanning electron microscope image of the area within the yellow dotted line in Fig. 2(a).

3. Results and discussion

Figure 3(a) illustrates the band diagrams of the two photonic structures used in the device, which were obtained using a photonic band microscope via hyperspectral Fourier image spectroscopy [27]. During the measurement, light from a broadband white light source was incident on the device, and a Fourier image of the scattered light was captured using an infrared camera through a 4f optical system. A tunable filter was placed in front of the infrared camera, and the three-dimensional (3D) photonic band was obtained by stacking the Fourier images captured at each wavelength in the 3D direction. Figure 3(a) indicates that the band gaps in both band diagrams are close to 1.55 μm, which is the optical communication wavelength band; however, their intensities at the upper and lower bandgap edges are reversed near the Γ point. In general, due to the difference in mode shape and phase distribution between *p*- and *d*-wave, the reflectivity of the electromagnetic mode of the *d*-wave tends to be weaker than that of the *p*-wave [19]. Therefore, the obtained experimental results indicate that the *p*-wave and *d*-wave electromagnetic modes are band-reversed, implying that the two photonic structures exhibit distinct topologies.

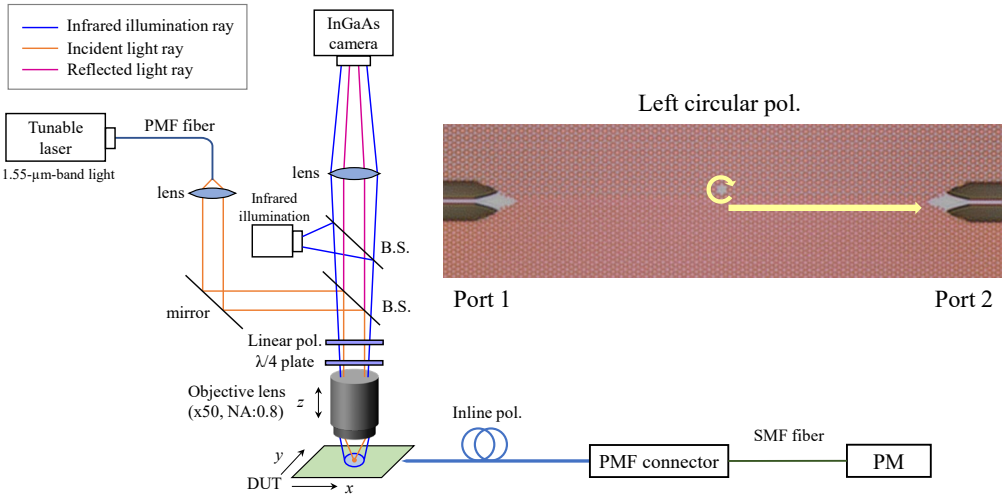

Fig. 3. (a) Measured band structure of photonic crystals with different topologies. (b) Basic transmission characteristics of the topological waveguide used in this study.

Optics EXPRESS

Figure 3(b) depicts the wavelength dependence of the propagation characteristics of the topological waveguide (without the defective structure) formed by the aforementioned two photonic structures. In the obtained band of the photonic structure (Fig. 3(a)), low-loss propagation of up to 0.10 dB/cell was recorded. Additionally, the spin–spin scattering resulted in an increase in the propagation loss in the vicinity of 1580–1590 nm near the bandgap center. These results indicate that the topological waveguide was appropriately configured.

We then measured the changes in vertical coupling efficiency with and without the defect structure based on the aforementioned topological waveguide. Figure 4 depicts the experimental setup. During the experiment, the light from a tunable laser was passed through a polarization-maintaining fiber and collimating lens. Subsequently, a plane wave of left or right circular polarization was generated using a polarizer and λ/4 wave plate. The light was then input from the top of the device by an objective lens (Olympus MPLFLN50 ×; numerical aperture = 0.8). The incident light was aligned with the center of the defect structure by monitoring the infrared camera placed above the device. The light propagated through the topological waveguide was output to a polarization-maintaining fiber via a ball-tip fiber from the end face of the device. Subsequently, the propagation characteristics were evaluated using a spectrum analyzer and power monitor. To eliminate stray light and extract only the light that has propagated through the topological waveguide, an in-line polarizer was inserted into the polarization-maintaining fiber on the output side to slice the E_y component. This component could not maintain the propagation mode at the interface between the two photonic structures with different topologies.

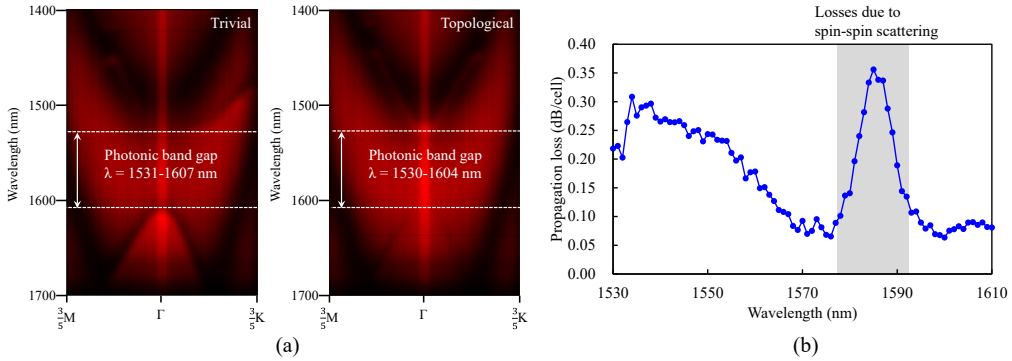

Fig. 4. Experimental setup. The circular polarization state of the vertically incident light is controlled using a linear polarizer and λ/4 wave plate.

Figure 5(a) illustrates the wavelength dependence of the output intensity of port 2 when left-handed circularly polarized light is incident. Here the output intensity was obtained by subtracting the coupling loss of the topological converter, the propagation loss of the Si wire waveguide, the coupling loss between the tip end face and the lensed fiber, and the insertion loss of the measurement system from the intensity actually measured with the power monitor, thereby extracting only the properties of topological waveguides with defect structures. In the band region with the topological edge state, the vertically incident light was more strongly coupled with the waveguide that comprised the defect structure compared with the one without the defect structure. Based on the results in Fig. 5(a), we plotted the wavelength dependence of the coupling efficiency enhancement ratio induced by the defect structure (Fig. 5(b)), which was determined by dividing the coupling efficiency obtained for the waveguide with the defect structure by that obtained for the waveguide without the defect structure. The figure indicates a performance improvement of up to 10 dB in the operating wavelength band of the defect structure (1550–1580 nm). The theoretical details on wavelength dependence of defect structures are presented in [24].

Optics EXPRESS

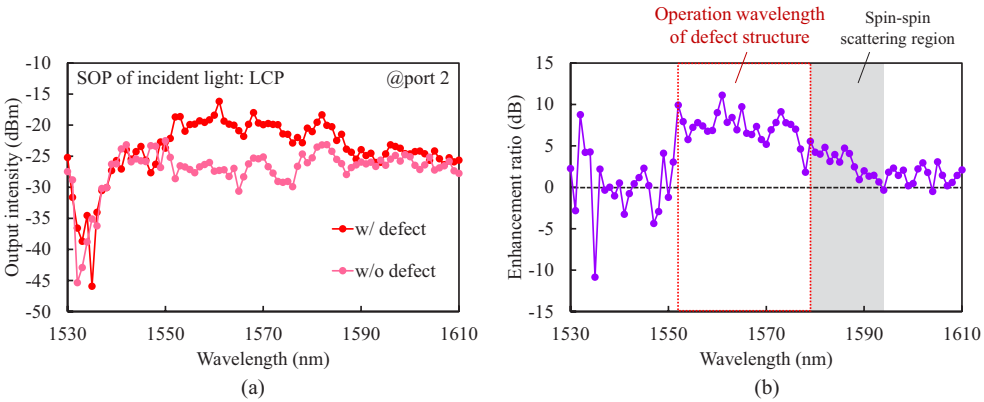

Fig. 5. (a) Wavelength dependence of output intensity with respect to the vertically incident light and topological waveguide with and without the defect structure. (b) Output intensity enhancement ratio induced by the defect structure.

Figure 6 depicts the wavelength dependence of the output intensity considering the loss of the measurement system from both ports when right- and left-handed circularly polarized lights are incident on the device. Figure 6(a) indicates that the observed output intensities from the same port reveal a phenomenon unique to topological waveguides in the case of both right- and left-handed circularly polarized lights. Here, the outputs to ports 1 and 2 are dominant when the incident light is right- and left-handed circularly polarized, respectively. In the operating wavelength band of the defect structure, the output intensity ratio between ports 1 and 2 was up to approximately 20 dB. Note that there is no change in the directionality of coupling with or without defects, and that the contrast ratio for left and right circular polarization is almost identical. Figure 6(b) depicts the output intensities from the ports where both the left- and right-handed circularly polarized lights are dominant. As the propagation characteristics obtained for both circular polarizations are similar, these results indicate that the introduced defect structure operates well for both circular polarizations.

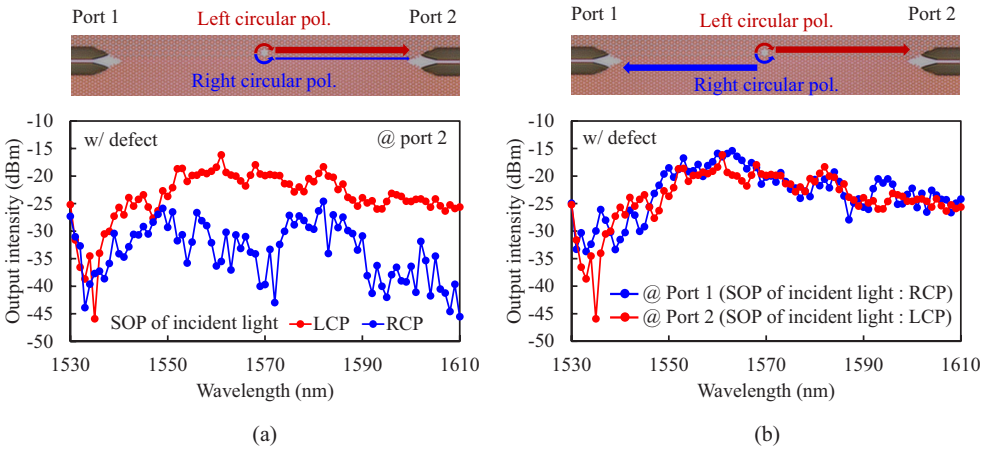

Fig. 6. Propagation characteristics of the topological waveguide with the defect structure when left- and right-handed circularly polarized lights are incident. Measurement results for (a) port1 only and (b) both ports.

Optics EXPRESS

4. Conclusions

In this study, we introduced a defect structure to achieve highly efficient vertical coupling in a topological waveguide. The topological waveguide was constructed by triangle lattices of hexagons consisting of six nanoholes respecting C_{6v} symmetry. The defect structure was introduced by removing the triangular nanoholes from one cell near the waveguide and by adding a dielectric material with a high refractive index. We fabricated an actual device to evaluate its coupling efficiency with and without this defect structure. Our analysis determined that the introduced defect structure operates suitably for both left- and right-handed circularly polarized lights, enhancing the performance in the optical communication wavelength bandwidth by up to 10 dB. The proposed uniform structure provides highly efficient coupling in the vertical direction when light is incident from free space to the topological photonics region in waveguides, aiding the implementation of TPICs.

Funding. Ministry of Education, Culture, Sports, Science and Technology (JPMXP1222IT0027); Japan Society for the Promotion of Science (#22H01520); Adaptable and Seamless Technology Transfer Program through Target-Driven R and D (JPMJTR22RG); Core Research for Evolutional Science and Technology (JPMJCR18T4).

Disclosures. The authors declare no conflicts of interest.

Data availability. No data were generated or analyzed in the presented research.

References

1. M. Z. Hasan and C. L. Kane, "Colloquium: topological insulators," Rev. Mod. Phys. **82**(4), 3045–3067 (2010).
2. X. L. Qi and S. C. Zhang, "Topological insulators and superconductors," Rev. Mod. Phys. **83**(4), 1057–1110 (2011).
3. H. Weng, R. Yu, and X. Hu, *et al.*, "Quantum anomalous Hall effect and related topological electronic states," Adv. Phys. **64**(3), 227–282 (2015).
4. Z. Wang, Y. Chong, and J. D. Joannopoulos, *et al.*, "Observation of unidirectional backscattering-immune topological electromagnetic states," Nature **461**(7265), 772–775 (2009).
5. L.-H. Wu and X. Hu, "Scheme for achieving a topological photonic crystal by using dielectric material," Phys. Rev. Lett. **114**(22), 223901 (2015).
6. T. Ozawa, H. M. Price, and A. Amo, *et al.*, "Topological photonics," Rev. Mod. Phys. **91**(1), 015006 (2019).
7. J. D. Joannopoulos, P. R. Villeneuve, and S. Fan, "Photonic crystals: putting a new twist on light," Nature **386**(6621), 143–149 (1997).
8. T. Baba, "Slow light in photonic crystals," Nat. Photonics **2**(8), 465–473 (2008).
9. K. Kondo, T. Tatebe, and S. Hachuda, *et al.*, "Fan-beam steering device using a photonic crystal slow-light waveguide with surface diffraction grating," Opt. Lett. **42**(23), 4990–4993 (2017).
10. T. Asano, Y. Ochi, and Y. Takahashi, *et al.*, "Photonic crystal nanocavity with a Q factor exceeding eleven million," Opt. Express **25**(3), 1769–1777 (2017).
11. J. B. Pendry, A. J. Holden, and D. J. Robbins, *et al.*, "Magnetism from conductors and enhanced nonlinear phenomena," IEEE Trans. Microwave Theory Tech. **47**(11), 2075–2084 (1999).
12. R. A. Shelby, D. R. Smith, and S. Schultz, "Experimental verification of a negative index of refraction," Science **292**(5514), 77–79 (2001).
13. T. Amemiya, T. Shindo, and D. Takahashi, *et al.*, "Nonunity permeability in metamaterial-based GaInAsP/InP multimode interferometers," Opt. Lett. **36**(12), 2327–2329 (2011).
14. N. I. Zheldev and Y. S. Kivshar, "From metamaterials to metadevices," Nat. Mater. **11**(11), 917–924 (2012).
15. T. Amemiya, T. Kanazawa, and S. Yamasaki, *et al.*, "Metamaterial waveguide devices for integrated optics," Materials **10**(9), 1037 (2017).
16. T. Amemiya, S. Yamasaki, and M. Tanaka, *et al.*, "Demonstration of slow-light effect in silicon-wire waveguides combined with metamaterials," Opt. Express **27**(10), 15007–15017 (2019).
17. M. Tanaka, T. Amemiya, and H. Kagami, *et al.*, "Control of slow-light effect in a metamaterial-loaded Si waveguide," Opt. Express **28**(16), 23198–23208 (2020).
18. M. Kim, Y. Kim, and J. Rho, "Spin-valley locked topological edge states in a staggered chiral photonic crystal," New J. Phys. **22**(11), 113022 (2020).
19. N. Parappurath, F. Alpeggiani, and L. Kuipers, *et al.*, "Direct observation of topological edge states in silicon photonic crystals: Spin, dispersion, and chiral routing," Sci. Adv. **6**(10), eaaw4137 (2020).
20. S. Peng, N. J. Schilder, and X. Ni, *et al.*, "Probing the band structure of topological silicon photonic lattices in the visible spectrum," Phys. Rev. Lett. **122**(11), 117401 (2019).
21. D. Smirnova, S. Kruk, and D. Leykam, *et al.*, "Third-harmonic generation in photonic topological metasurfaces. Physical review letters," Phys. Rev. Lett. **123**(10), 103901 (2019).
22. H. Kagami, T. Amemiya, and S. Okada, *et al.*, "Selective excitation of optical vortex modes with specific charge numbers in band-tuned topological waveguides," Opt. Lett. **47**(9), 2190–2193 (2022).

Optics EXPRESS

23. N. Badraoui and T. Berceli, "Enhancing capacity of optical links using polarization multiplexing," Opt. Quantum Electron. **51**(9), 310 (2019).
24. H. Kagami, T. Amemiya, and S. Okada, *et al.*, "Highly efficient vertical coupling to a topological waveguide with defect structure," Opt. Express **29**(21), 32755–32763 (2021).
25. S. Okada, T. Amemiya, and H. Kagami, *et al.*, "Discussion on fabrication accuracy of infrared topological photonic structures using hyperspectral Fourier image spectroscopy," J. Opt. Soc. Am. B **39**(9), 2464–2469 (2022).
26. H. Kagami, T. Amemiya, and S. Okada, *et al.*, "Topological converter for high-efficiency coupling between Si wire waveguide and topological waveguide," Opt. Express **28**(22), 33619–33631 (2020).
27. T. Amemiya, S. Okada, and H. Kagami, *et al.*, "High-speed infrared photonic band microscope using hyperspectral Fourier image spectroscopy," Opt. Lett. **47**(10), 2430–2433 (2022).